Supporting Information

Jacobson and Archer 10.1073/pnas.1208993109

SI Text

SI Materials and Methods. The model used for this study was GATOR-GCMOM, a global-through-urban nested model (1–3). The model was modified to treat wind turbines as an elevated sink of momentum, where the kinetic energy extracted from the wind is determined from a turbine power curve at the instantaneous model wind speed. The treatment of turbines developed here is similar in concept to that of *Baidya Roy* (4, 5) but differs in the following ways: it (*i*) assumes each wind turbine occupies multiple vertical atmospheric layers rather than one layer, (*ii*) is applied to numerous wind farms worldwide simultaneously rather than one local farm, (*iii*) is applied in a global model where momentum extraction feeds back to global dynamics rather than a limited-area model with only regional feedbacks, and (*iv*) accounts for the conservation of energy due to both electricity use and turbulent dissipation of kinetic energy. In addition, the new treatment allows distributed wind turbines in a grid cell to extract energy from a staggered Arakawa C grid rather than from the center of the cell. With the C grid, u, and v are located at grid cell edges. As such, turbines distributed throughout a grid cell alter wind speeds at four locations in the cell rather than at one central location. Because cell edges join two cells, wind speed changes with the C grid affect five cells simultaneously rather than one.

The treatment of kinetic energy extraction by wind turbines in the model is described as follows. Each turbine is characterized by a rated power [P_t, 5 megawatts (MW)], a rotor diameter (D, 126 m), a hub height above the topographical surface (H, 100 m), and a characteristic spacing area (m^2) $A_t = xD \times yD$, usually determined by convention to minimize interference of the wake of one turbine with the next turbine. In this equation, x and y are constants that provide distances perpendicular to and parallel to, respectively, the prevailing wind direction. Some values used previously have been $x = 4$, $y = 7$; $x = 3$, $y = 10$ (6).

Each model grid cell contains a specified number of turbines. The maximum number of turbines in the grid cell is $N_t = A_c/A_t$, where A_c is the ground area occupied by the cell (m^2).

For determining extraction of energy, each turbine is assumed to intersect one or more atmospheric layers of a grid column. This configuration applies regardless of whether the turbines exist in the boundary layer or jet stream and for either global or regional domains. The configuration requires modification only when the horizontal resolution of the model $< D (= 126$ m in the present application). All simulations here were run at coarser horizontal resolution than this resolution.

The momentum extracted from each layer k that the turbine intersects is proportional to the ratio of the swept area of the turbine residing in the layer (S_k) divided by the total swept area (m^2) of the turbine, $S_t = \pi D^2/4$. The swept area residing in a layer is determined from geometry. For example, the swept area falling in the lowest layer of Fig. S1 (ABCDA) is the area HADCH minus the area HABCH. Because the hub height (point H) and the height above the ground of the edge of each layer (e.g., point B) are known, the vertical distance HB is also known. Because the distance HC, which is the turbine radius $R = D/2$, is also known, the angle BHC is $\theta_{BHC} = \arccos(HB/R)$. Therefore, area $HADCH = 2\theta_{BHC} S_t/2\pi$, and area $HABCH = HB \times R \sin(\theta_{BHC})$. The areas of subsequent layers are calculated from bottom to top in a similar manner, taking into account the summed areas determined already.

Kinetic energy is extracted from each model layer that intersects the turbine rotor each time step Δt due to conversion of the kinetic energy to electric power by the turbine. The global and regional domains in the model use the Arakawa C grid structure; thus, u scalar velocities are located at the west $(i-1/2, j)$ and east $(i+1/2, j)$ edges of each grid cell in each layer k, v scalar velocities are located at the south $(i, j-1/2)$ and north $(i, j+1/2)$ edges, and mass M (kg) and other scalars are located at the center (i, j, k) of the cell. As such, the initial (subscript I) total kinetic energy in grid cell i, j, k before energy extraction is

$$E_{\mathrm{I},i,j,k} = 0.5(E_{\mathrm{I},i-1/2,j,k} + E_{\mathrm{I},i+1/2,j,k} + E_{\mathrm{I},i,j-1/2,j,k} + E_{\mathrm{I},i,j+1/2,j,k}). \quad \text{[S1]}$$

In this equation,

$$\begin{aligned} E_{\mathrm{I},i-1/2,j,k} &= 0.5 M_{i-1/2,j,k} u^2_{\mathrm{I},i-1/2,j,k}, \\ &\text{where } M_{i-1/2,j,k} = 0.5(M_{i-1,j,k} + M_{i,j,k}) \\ E_{\mathrm{I},i+1/2,j,k} &= 0.5 M_{i+1/2,j,k} u^2_{\mathrm{I},i+1/2,j,k}, \\ &\text{where } M_{i+1/2,j,k} = 0.5(M_{i,j,k} + M_{i+1,j,k}) \\ E_{\mathrm{I},i,j-1/2,k} &= 0.5 M_{i,j-1/2,k} v^2_{\mathrm{I},i,j-1/2,k}, \\ &\text{where } M_{i,j-1/2,k} = 0.5(M_{i,j-1,k} + M_{i,j,k}) \\ E_{\mathrm{I},i,j+1/2,k} &= 0.5 M_{i,j+1/2,,k} v^2_{\mathrm{I},i,j+1/2,,k}, \\ &\text{where } M_{i,j+1/2,k} = 0.5(M_{i,j,k} + M_{i,j+1,k}). \end{aligned} \quad \text{[S2]}$$

The average horizontal wind speed at the vertical and horizontal center of a cell, used to determine kinetic energy extraction by a wind turbine to produce electricity, is thus $W_{i,j,k} = [2E_{\mathrm{I},i,j,k}/M_{i,j,k}]^{1/2}$. Each time step, the kinetic energy extracted from the turbine in a given cell is calculated as

$$\Delta E_{i,j,k} = P_{i,j,k} \Delta t S_k / S_t, \quad \text{[S3]}$$

where $P_{i,j,k}$ is the power extracted from the turbine at instantaneous wind speed $W_{i,j,k}$ based on its power curve. Eq. **S3** implies that the power determined from the power curve is calculated with a different wind speed in each model layer intersecting the turbine. Whereas power curves are derived based on the wind speed at hub height, the assumption of varying power extraction for varying heights in the turbine is necessary, because otherwise it would be possible to extract more energy from a layer than is physically present. For example, suppose (in a hypothetical extreme case), the wind speed were 0 m/s in the lowest layer intersecting the turbine and 10 m/s at hub height. Subtracting a portion of the total energy extracted from the lowest layer would be unphysical. Because wind speeds vary roughly logarithmically with height and the height of a turbine swept area is only D, higher wind power extracted at the turbine top are roughly compensated for by lower power extracted at the bottom. The error due to this assumption is likely less than the error due to that of the power curve, which is derived under neutrally stratified conditions in the absence of wind shear.

For the REPower 5-MW turbine, a fit to the power curve data, combined with a correction for air density, is

$$P_{i,j,k} = \frac{\rho_a(T,P,q)}{\rho_{a,\mathrm{STP}}} \begin{cases} 0 & W_{i,j,k} < 3.5002 \text{ m/s} \quad \text{or} \quad W_{i,j,k} > 30 \text{ m/s} \\ 807.69 + W_{i,j,k}(-495.51 + W_{i,j,k}(77.88 - 0.64 W_{i,j,k})) & 3.5002 \le W_{i,j,k} \le 10 \text{ m/s} \\ 12,800 + W_{i,j,k}(-5713.3 + W_{i,j,k}(740.0 - 26.667 W_{i,j,k})) & 10 < W_{i,j,k} \le 13 \text{ m/s} \\ 5000 & 13 < W_{i,j,k} \le 30 \text{ m/s} \end{cases} \quad \textbf{[S4]}$$

based on manufacturer-provided power output vs. wind speed, where $\rho_{a,\mathrm{STP}} = 1.225$ kg/m^3 is air density at standard temperature and pressure and $\rho_a(T,P,q)$ is air density at the current temperature (T), pressure (P), and specific humidity (q) in the model. The power curve indicates a cut-in wind speed of 3.5 m/s, a cut-out wind speed of 30 m/s, and a rated wind speed of 13 m/s.

The final kinetic energy in each grid cell is thus $E_{\mathrm{F},i,j,k} = E_{\mathrm{I},i,j,k} - \Delta E_{i,j,k}$. The turbine also converts some kinetic energy into turbulent kinetic energy (TKE), primarily in the vertical. This conversion is roughly accounted for in the model because the reduction in wind speed due to the turbine results in wind shear, creating subgrid-scale mechanical turbulence and TKE through a level 2.5 TKE closure scheme (7). The increase in TKE increases the turbulent diffusion coefficient for momentum, increasing the vertical transport of horizontal momentum down gradients (and reducing it up gradients) in the presence of the turbine-generated turbulence or large-scale shear- or buoyancy-driven turbulence in a second-order local closure diffusion calculation in the model. Energy, moisture, and trace chemicals are similarly transported across gradients due to turbulent diffusion. No treatment of constructive or destructive interference by wakes is introduced because wakes are not resolved at the scale of interest.

The change in total kinetic energy in the grid cell is next partitioned proportionately among the kinetic energies of the surrounding u and v points with

$$\begin{aligned} E_{\mathrm{F},i-1/2,j,k} &= E_{\mathrm{I},i-1/2,j,k} E_{\mathrm{F},i,j,k} / E_{\mathrm{I},i,j,k} \\ E_{\mathrm{F},i+1/2,j,k} &= E_{\mathrm{I},i+1/2,j,k} E_{\mathrm{F},i,j,k} / E_{\mathrm{I},i,j,k} \\ E_{\mathrm{F},i,j-1/2,k} &= E_{\mathrm{I},i,j-1/2,,k} E_{\mathrm{F},i,j,k} / E_{\mathrm{I},i,j,k} \\ E_{\mathrm{F},i,j+1/2,k} &= E_{\mathrm{I},i,j+1/2,,k} E_{\mathrm{F},i,j,k} / E_{\mathrm{I},i,j,k}. \end{aligned} \quad \textbf{[S5]}$$

The final wind speed at each u and v point is then

$$\begin{aligned} u_{\mathrm{F},i-1/2,j,k} &= \mathrm{sign}\left(\sqrt{2E_{\mathrm{F},i-1/2,j,k}/M_{i-1/2,j,k}}, u_{\mathrm{I},i-1/2,j,k}\right) \\ u_{\mathrm{F},i+1/2,j,k} &= \mathrm{sign}\left(\sqrt{2E_{\mathrm{F},i+1/2,j,k}/M_{i+1/2,j,k}}, u_{\mathrm{I},i+1/2,j,k}\right) \\ v_{\mathrm{F},i,j-1/2,k} &= \mathrm{sign}\left(\sqrt{2E_{\mathrm{F},i,j-1/2,k}/M_{i,j-1/2,k}} v_{\mathrm{I},i-1/2,j,k}\right) \\ v_{\mathrm{F},i,j+1/2,k} &= \mathrm{sign}\left(\sqrt{2E_{\mathrm{F},i,j+1/2,k}/M_{i,j+1/2,k}} v_{\mathrm{I},i+1/2,j,k}\right), \end{aligned} \quad \textbf{[S6]}$$

where sign() indicates that the sign of the final scalar velocity needs to be that of the initial value. Because each u and v point borders two grid cells, it is necessary to ensure that all grid cells are solved independently with initial wind speeds and that final u and v wind speeds at each border point are determined by adding differences from Eq. **S6**, such as $u_{\mathrm{F},i-1/2,j,k} - u_{\mathrm{I},i-1/2,j,k,}$ for both adjacent cells to the initial value, $u_{\mathrm{I},i-1/2,j,k}$, to obtain the final wind speed at the border point.

Energy conservation due to power generation and frictional dissipation of winds at the surface is maintained in the model by converting all electric power generated by the wind turbines to heat. The model also converts kinetic energy lost by natural surface roughness to turbulence and then heat. The electric power generated by turbines each time step, $\Delta E_{i,j,k}$, modifies the surface air temperature (where the electric power is consumed by human activity). Because the global model grid cells for the present simulations are large, it is assumed that the electricity is consumed in the same column that it is generated in. The temperature change (K) during a time step in surface layer *ksfc* due to electric power extraction in the model layers k between the bottom and top of a turbine rotor is

$$\Delta T_{i,j,ksfc} = \frac{1}{c_{p,m} M_{i,j,ksfc}} \sum_{k=\mathrm{bottom}}^{\mathrm{top}} \Delta E_{i,j,k}, \quad \textbf{[S7]}$$

where $c_{p,m}$ is the specific heat of moist air at constant pressure. Similarly the u- and v-components of kinetic energy lost due to friction and TKE generation at the topographical surface each time step are converted to internal energy and added to the temperature in the bottom model layer.

The model was initialized with 1° × 1° reanalysis meteorological fields (8) for simulations starting January 1, 2006 and run forward in time for five years with no data assimilation, as described in the main text. Oceans in the model were represented in 3D for some calculations and 2D for others. A 2D time-dependent mixed-layer ocean dynamics model driven by surface wind stress was used to solve for mixed-layer velocities, heights, and horizontal energy transport in each grid cell (9). The scheme conserves potential enstrophy, vorticity, energy, and mass and predicts gyres and major currents. Energy diffusion to the deep ocean was treated in 3D through 10 ocean layers below each surface grid cell. Air-ocean exchange, vertical diffusion through the ocean, and 3D ocean equilibrium chemistry and pH were solved as in (10).

Sea ice in the model could form on water surfaces, and snow could accumulate on sea ice. The model solved for the temperature at the ice-ocean interface, the snow-ice interface, the air-snow interface, and the air-ice interface as in (1), which assumed single layers of sea ice and snow on top of sea ice whose thicknesses were solved for over time. When the weight of sea ice plus snow caused the sea ice to submerge below sea level, snow was converted to sea ice. Although snow on top of sea ice was treated as one layer, the vertical density profile in the layer was calculated and other properties of snow varied with density. For permanent snow over land, the 10-layer subsurface model was used to transport energy through snow. Snow densities were calculated as a function of depth, and other properties varied with density. For all snow, sea ice, and water surfaces, an additional layer was added to the bottom of the atmospheric radiative transfer calculation to solve for radiation fluxes through snow, ice, and water, respectively. The purpose of adding this layer was to predict, rather than prescribe, the albedo at the snow-air, ice-air, and water-air interface, particularly in the presence of pollutants such as black carbon, brown carbon, and soil dust.

Fig. S2 compares near-surface wind speed predictions at 4 × 5 degree resolution from the model with 1.5 × 1.5 degree resolution data over the oceans. Despite the nine times coarser resolution of the model relative to the data, the model picked up the main features of the data. Some other comparisons of model behavior over the ocean can be seen in figure 2 of ref. 11, which compares modeled monthly sea ice area over the Antarctic and Arctic with data, and figure 2 of ref. 12, which compares modeled zonally averaged (from the surface to 18 km) static stability with satellite data. Static stability accounts for the vertical temperature profile.

1. Jacobson MZ (2001) GATOR-GCMM: A global- through urban-scale air pollution and weather forecast model. 1. Model design and treatment of subgrid soil, vegetation, roads, rooftops, water, sea ice, and snow. *J Geophys Res* 106:5385–5402.
2. Jacobson MZ, Wilkerson JT, Naiman AD, Lele SK (2011) The effects of aircraft on climate and pollution. Part I: Numerical methods for treating the subgrid evolution of discrete size- and composition-resolved contrails from all commercial flights worldwide. *J Comp Phys*230:5115–5132.
3. Jacobson MZ, Ten Hoeve JE (2012) Effects of urban surfaces and white roofs on global and regional climate. *J Climate* 25:1028–1044.
4. Baidya Roy S, Pacala SW, Walko RI (2004) Can large wind farms affect local meteorology. *J Geophys Res*109:D19101.
5. Baidya Roy S (2011) Simulating impacts of wind farms on local hydrometeorology. *J Wind Eng Ind Aerod*. 99:491–498.
6. Masters GM (2004) *Renewable and Efficient Electric Power Systems*. John Wiley & Sons, Hoboken, NJ.
7. Mellor GL, Yamada T (1982) Development of a turbulence closure model for geophysical fluid problems. *Rev Geophys Space Phys* 20:851–875.
8. Global Forecast System (GFS) weather reanalysis fields (2010) National Oceanic and Atmospheric Administration, Available at http://nomads.ncdc.noaa.gov/data/gfs-avn-hi/. Accessed February 23, 2012.
9. Ketefian GS, Jacobson MZ (2009) A mass, energy, vorticity, and potential enstrophy conserving boundary treatment scheme for the shallow water equations. *J Comp Phys* 228:1–32.
10. Jacobson MZ (2005) Studying ocean acidification with conservative, stable numerical schemes for nonequilibrium air-ocean exchange and ocean equilibrium chemistry. *J Geophys Res* 110:D07302.
11. Jacobson MZ (2010) Short-term effects of controlling fossil-fuel soot, biofuel soot and gases, and methane on climate, Arctic ice, and air pollution health. *J Geophys Res* 115:D14209.
12. Whitt DB, Wilkerson JT, Jacobson MZ, Naiman AD, Lele SK (2011) Vertical mixing of commercial aviation emissions from cruise altitude to the surface. *J Geophys Res*, 116:D14109.

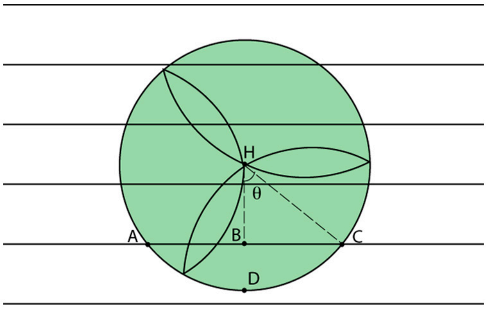

Fig. S1. Illustration of how the swept area of a single wind turbine intersects multiple model vertical layers in a single grid column. Points A, B, C, D, and H are discussed in the text.

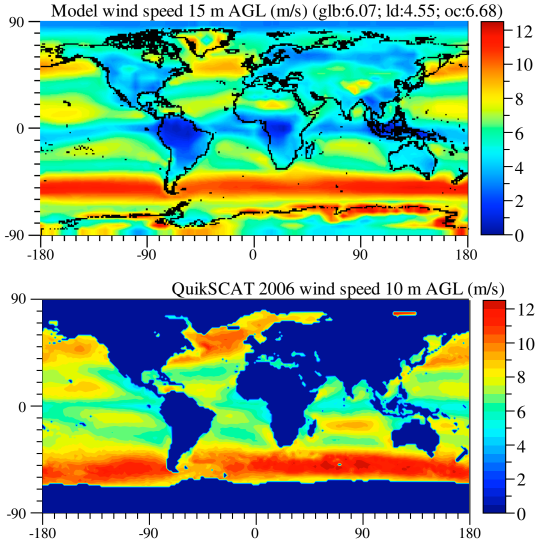

Fig. S2. Modeled 2006 15-m wind speed at 4×5 degree resolution vs. 10-m data at 1.5×1.5 degree resolution (1) for the same year.

1 *Quikscat* processed by Whitt D, Dvorak M (2010). Available at http://podaac.jpl.nasa.gov/DATA_CATALOG/quikscatinfo.html. Accessed February 23, 2012.

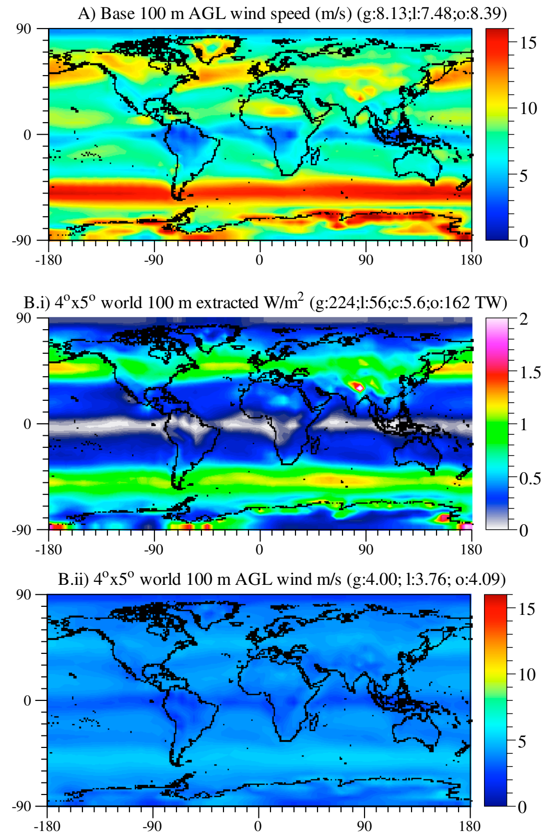
A) Base 100 m AGL wind speed (m/s) (g:8.13;l:7.48;o:8.39)
90
0
-90
-180
-90
0
90
180
15
10
5
0
B.i) 4°x5° world 100 m extracted W/m² (g:224;l:56;c:5.6;o:162 TW)
90
0
-90
-180
-90
0
90
180
2
1.5
1
0.5
0
B.ii) 4°x5° world 100 m AGL wind m/s (g:4.00; l:3.76; o:4.09)
90
0
-90
-180
-90
0
90
180
15
10
5
0

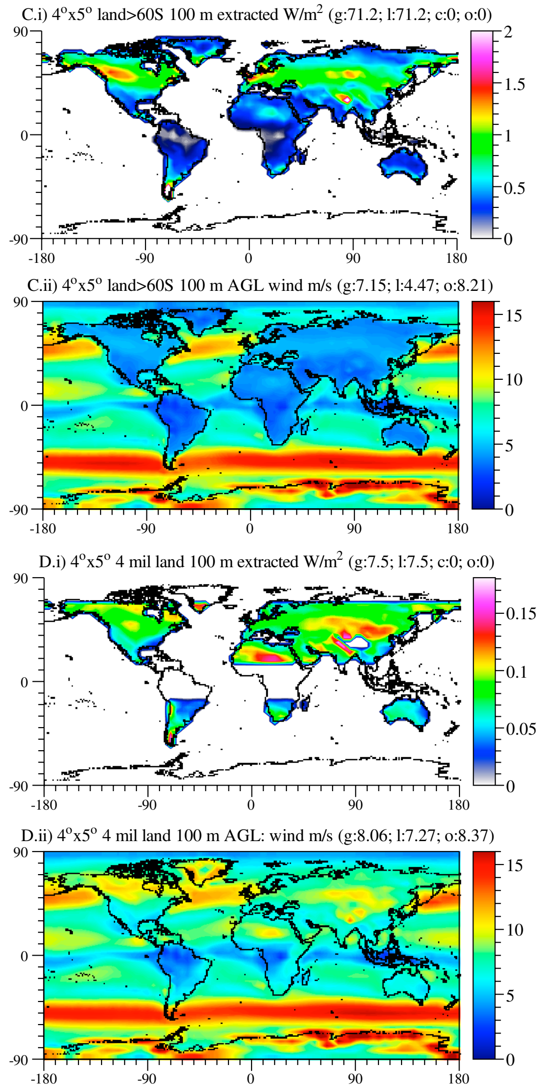
C.i) 4°x5° land>60S 100 m extracted W/m² (g:71.2; l:71.2; c:0; o:0)
C.ii) 4°x5° land>60S 100 m AGL wind m/s (g:7.15; l:4.47; o:8.21)
D.i) 4°x5° 4 mil land 100 m extracted W/m² (g:7.5; l:7.5; c:0; o:0)
D.ii) 4°x5° 4 mil land 100 m AGL: wind m/s (g:8.06; l:7.27; o:8.37)

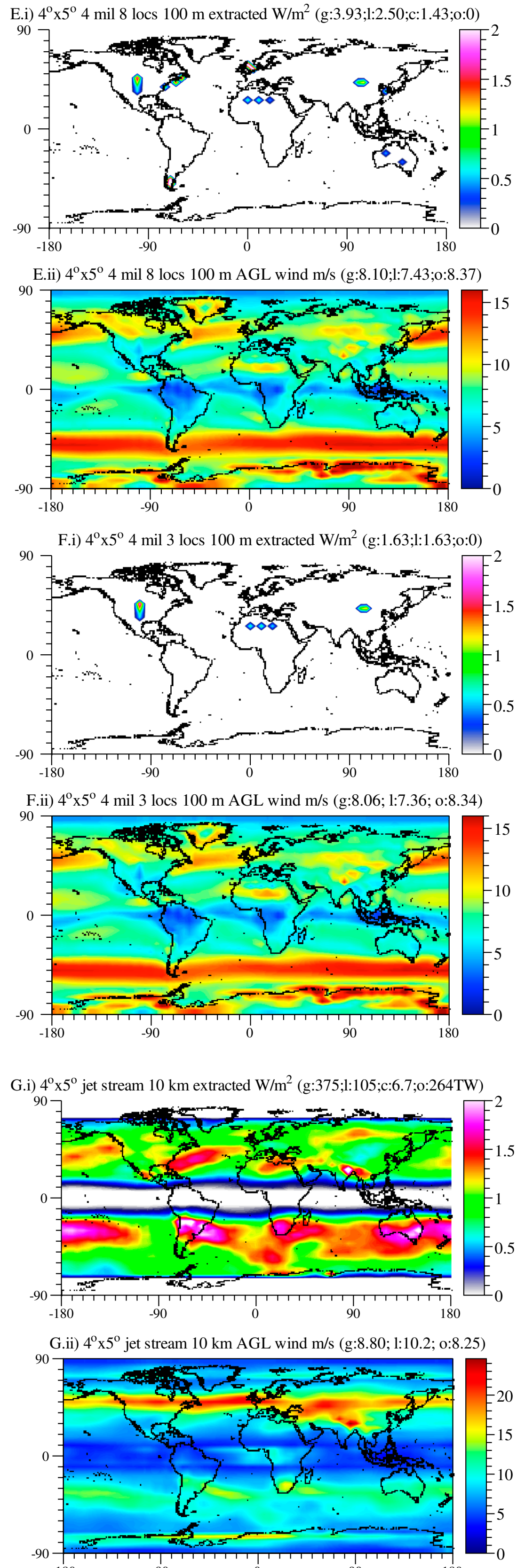

Fig. S3. (*A*) Modeled (4° × 5° horizontal resolution) annually-averaged (during the last year of simulation) 100-m wind speeds in the absence of wind turbine power extraction (Simulation A). (*B*) Same as (*A*) but for power (W/m²) extracted from wind turbines (*i*) and the resulting wind speeds (m/s) (*ii*) accounting for worldwide turbine momentum extraction (Simulation B). (*C*) Same as (*B*) but for wind turbines over all land outside Antarctica (Simulation I). (*D*–*F*) Same as (*B*) but for the three cases of four million turbines (Simulation N–P), (*G*) Same as (*B*) but for turbine extraction in the jet stream at 10 km (Simulation Q). g = global average; l = land-average; c = average over coastal ocean (water with depth less than 200 m outside Antarctica), and o = average over all other ocean.

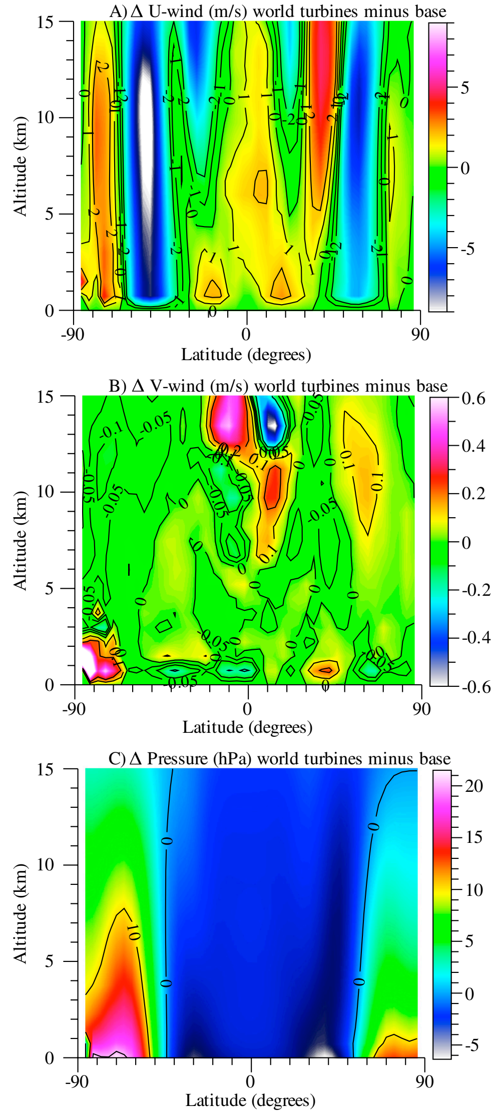

Fig. S4. Zonally averaged changes during the last simulation year in several meteorological variables between the global surface turbine case (Simulation B) and the base case (Simulation A).

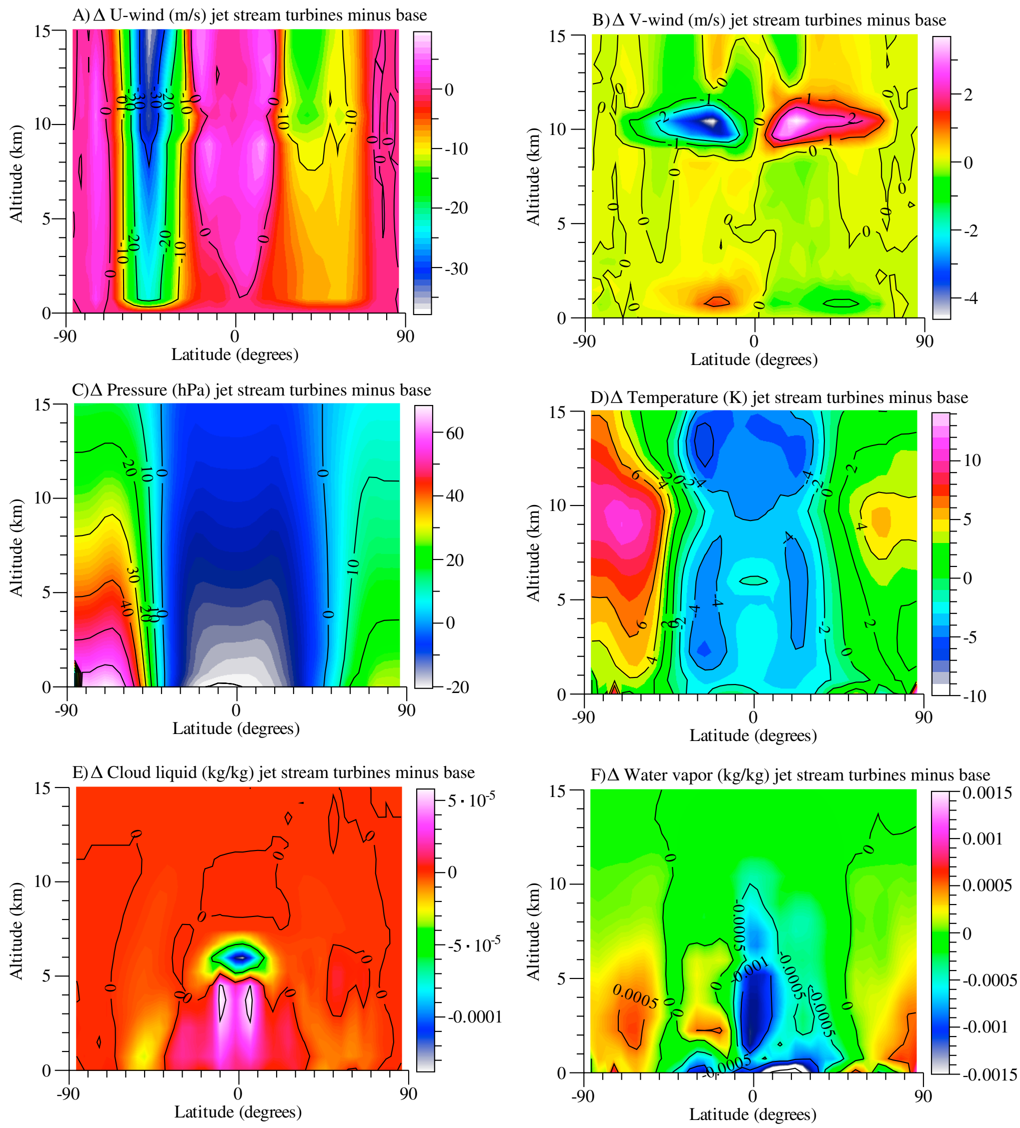

Fig. S5. Zonally averaged changes during the last simulation year in several meteorological variables between the case with turbines at 10 km (jet stream case, Simulation Q) and the base case (Simulation A).